Available online at www.sciencedirect.com

ScienceDirect

Procedia Materials Science 3 (2014) 1872 – 1877

Procedia Materials Science

www.elsevier.com/locate/procedia

20th European Conference on Fracture (ECF20)

Site-bond modelling of structure-failure relations in quasi-brittle media

Andrey P Jivkov*, Mingzhong Zhang, Craig N Morrison

Mechanics and Physics of Solids Research Team, School of Mechanical, Aerospace and Civil Engineering, The University of Manchester, Oxford Road, Manchester, M13 9PL, UK

Abstract

The non-linear behaviour of quasi-brittle media emerges from distributed micro-cracking. This is analysed conveniently by discrete lattice models. A 3D site-bond model is specialised here for materials with three-phase microstructures: stiff inclusions in a compliant matrix containing pores. The deformation behaviour is based on analytically derived relations between bond properties, length scale and macroscopic elastic constants. The microstructure-model mapping is based on size distributions and volume densities of inclusions and pores, typically obtained through analyses of 3D images. Inclusions data is used to calculate the required length scale. Pores data is used to define the failure behaviour of individual bonds. Applications of the methodology to cement-based materials and nuclear graphite are presented separately in this volume.

Selection and peer-review under responsibility of the Norwegian University of Science and Technology (NTNU), Department of Structural Engineering

Keywords: Quasi-brittle material; Lattice-spring model; Microstructure; Elastic behaviour; Local damage.

1. Introduction

Quasi-brittle materials, such as cements, rocks and graphite, are characterised by elastic-brittle behaviour at the length-scale of their microstructure features and non-linear behaviour preceding failure at the engineering length-scale. The cause for this "gracefulness" is the generation of micro-cracks which, in contrast to ideally brittle media,

* Corresponding author. Tel.: +44-161-306-3765; fax: +44-161-200-3723.
E-mail address: andrey.jivkov@manchester.ac.uk

Selection and peer-review under responsibility of the Norwegian University of Science and Technology (NTNU), Department of Structural Engineering
doi:10.1016/j.mspro.2014.06.302

dissipates strain energy and reduces the apparent elastic modulus progressively. The modelling of spatially distributed micro-cracking and the analysis of its effect on the longer-scale behaviour can provide insights into the microstructure-failure relations. For a given material with fixed microstructure, this would improve our understanding of the damage evolution ahead of a macroscopic crack, with a potential to derive mechanistic constitutive laws for continuum damage modelling of fracture. In the first instance, the modelling can provide an estimate for the size of the fracture process zone for given microstructure, which in quasi-brittle media could be defined as the energy dissipating 3D region. This is important since the parameters controlling this size are still not clearly understood. For example, according to Awaji et al (2010) and Aliha and Ayatollahi (2012) the size of the fracture process zone scales with the squared ratio of the fracture toughness and tensile strength. However, Ayatollahi and Aliha (2011) have pointed out that the size could be related to the average grain size alone. Further, such modelling could be used for predicting changes in longer- or engineering scale behaviour with service-related changes in the microstructure geometry, topology and properties, as pointed out by Jivkov et al (2013a). For example, geometry and connectivity changes of the pore space due to corrosion/erosion and changes of local mechanical properties of the solid phases due to chemical reactions.

Discrete lattice models provide a convenient framework for analysis of distributed micro-cracking, with interactions and coalescences controlled solely by applied loads and locally evolving microstructure. Lattices have generating cellular architecture, where sites located in cells are linked by bonds resisting relative deformations between cells. The relation between bond properties and continuum response can be established either by relating bond forces to cell stresses, as shown e.g. by Carol et al. (2001) and Cusatis et al. (2011), or by equating the strain energy in the bonds and the cell, as shown e.g. by Griffiths and Mustoe (2001) and Karihaloo et al. (2003). The latter can be used for deriving explicit bond-continuum relations for regular cellular architectures. This is useful, because regular lattices can be considered to represent topologically homogenised microstructures and offer high computational efficiency compared to irregular, i.e. image-based, lattices. Rigorous derivation of bond properties, represented as bundles of one normal and two shear springs, performed by Wang and Mora (2008), showed that for the most widely used 2D lattice with hexagonal generating cell a requirement for positive spring stiffness limits the applicability of the lattice to isotropic materials with Poisson's ratio of up to 1/4 in plane strain and up to 1/3 in plane stress. Further for 3D lattices based on HCP and FCC arrangements it was shown that only isotropic materials with zero Poisson's ratio could be represented. This holds also for simple cubic lattice. As a result, mechanically realistic simulations of micro-cracking have been mainly performed on 2D hexagonal structures, e.g. Schlangen and van Mier (1992) and Liu et al. (2009). Real crack morphologies, however, are intrinsically non-planar and an appropriate lattice is required to capture crack spatial evolution.

A novel lattice, based on a compact tessellation of space into truncated octahedral cells, was proposed recently by Jivkov and Yates (2012). With bonds represented by beams, this lattice was shown numerically to reproduce any isotropic material of practical interest, in contrast to previously used lattices. The beam-based lattice with elastic-brittle local behaviour has been used to simulate the response of concrete under complex triaxial loading, as reported by Jivkov et al. (2013b). The beams, however, introduce local micropolar effect, which does not allow for closed form calibration of beam properties without assuming generalised elasticity in cells and the knowledge of the curvature-couple-stress constitutive relations; details on required additional material parameters can be found in Hadjesfandiari and Dargush (2011).

Following Wang and Mora (2008), assuming classical continuum in cell and bonds represented by one normal and two shear springs, Zhang et al. (2014a) derived a closed form relation between spring constants and macroscopic elastic constants for the new lattice. This derivation will be presented here briefly to facilitate discussion on the meaning of different parameters and their link to microstructure features. The emphasis will then be on the mapping of the microstructure characteristics to the spring-lattice. We call a lattice made correspondent to a microstructure, the site-bond model of the material. This work specialises the site-bond model to three-phase quasi-brittle media: stiff inclusions in a compliant matrix containing pores. In such case inclusions occupy cells, i.e. coincide with lattice sites, and bonds represent matrix deformation with potential for failure dependent on distributed porosity. The microstructure information required for such correspondence are the size distribution and volume densities of inclusions and pores. Successful applications of the methodology are presented separately for cement-based materials by Zhang et al (2014b), and for nuclear graphite by Morrison et al. (2014a, b).

2. Lattice elasticity

Material volume is represented by a complex of compactly packed identical cells – truncated octahedrons; one cell is shown in Fig. 1. This is an a priory topological homogenisation since the proposed cell is closest to the average cell in a random Voronoi tessellation of space, see Jivkov and Yates (2012) for details, hence most suitable for describing neighbourhoods of material features in average. In the material volume complex, cells are allowed to undergo topological transformations only, i.e. to deform without cutting. Discontinuities are allowed on the faces between cells, i.e. micro-cracks may emerge and propagate between cells. One important advantage of the proposed complex is that it allows for richer and more realistic crack morphology than previously studied 3D lattices.

Lattice-based models reduce cell complexes to site-bond structures following partially the construction of a dual complex, where nodes, edges, faces and cells correspond to cells, faces, edges and nodes, respectively, of the primal complex. The reduction terminates the construction after sites (nodes) and bonds (edges) of the dual complex are assigned. Notably, the sites and bonds inherit geometric characteristics from the primal complex, namely volume and area, with added mechanical functions to displace and resist relative displacements, respectively. The proposed cell has six neighbours along three orthogonal directions (±1, 0, 0), (0, ±1, 0), (0, 0, ±1) and eight neighbours along the body diagonals (±1, ±1, ±1), where all sign combinations are taken. The cell size, S, is selected to be the distance between two opposite square faces, thus the cell volume is $V = S^3/2$, the hexagonal face area is $A_1 = S^2 3\sqrt{3}/16$, and the square face area is $A_2 = S^2/8$. The reduction leads to 14 bonds of two types, one normal to hexagonal faces (nearer neighbours) denoted by B_1 with length $L_1 = S\sqrt{3}/2$ and one normal to square faces (further neighbours) denoted by B_2 with length $L_2 = S$; one of each type is shown in Fig. 2.

The bond resistance to relative displacements between adjacent sites is represented by one axial (normal to cell face) and two transverse (tangent to cell face) springs, forming a proper orthogonal system. The two transverse springs in a bond have identical stiffness. Thus the lattice interactions are characterised by four constants, K_1, T_1, K_2, T_2, the stiffness coefficients of axial and transverse springs in bonds B_1 and B_2, respectively. These constants are determined by equating the energy in a continuum cell and half the energy in the 14 bonds, assuming a locally linear displacement field, $u_i = \varepsilon_{ij} x_i$, i.e. a homogeneous strain field ε_{ij}, as in Wang and Mora (2008). Under this assumption the strain energy in the cell is calculated by Eq. (1) where C_{ijkl} are the components of the elasticity tensor. The strain energy in the springs within the cell is given by Eq. (2) where $\Delta_{i,b}$ stands for the relative displacement of the bond ends in its local coordinate system as given above.

$$U_c = \frac{1}{2}\int_{Cell} C_{ijkl}\varepsilon_{ij}\varepsilon_{kl}\,dv = \frac{S^3}{4} C_{ijkl}\varepsilon_{ij}\varepsilon_{kl} \tag{1}$$

$$U_d = \frac{1}{4}\sum_{B_1}\left[K_1\Delta_{1,b}^2 + T_1\left(\Delta_{2,b}^2 + \Delta_{3,b}^2\right)\right] + \frac{1}{4}\sum_{B_2}\left[K_2\Delta_{1,b}^2 + T_2\left(\Delta_{2,b}^2 + \Delta_{3,b}^2\right)\right] \tag{2}$$

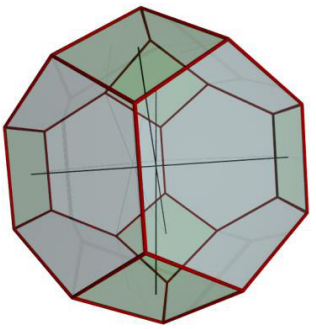

Fig. 1. Unit cell of cellular complex.

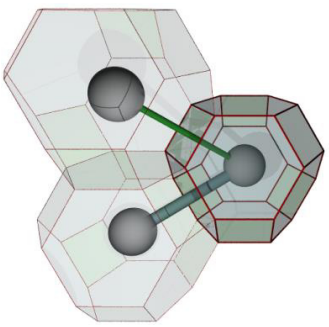

Fig. 2. Elements of discrete lattice.

By expressing relative displacements via strains and accounting for bond lengths, the following relations are found (for detailed derivation see Zhang et al., 2014a)

$$C_{iiii} = \frac{2}{3S}\left(K_1 + 2T_1 + 3K_2\right), \quad for\ i = 1,2,3 \tag{3}$$

$$C_{iijj} = \frac{2}{3S}\left(K_1 - T_1\right), \quad for\ i \neq j\ and\ i,j = 1,2,3 \tag{4}$$

$$C_{ijij} = \frac{2}{3S}\left(K_1 + 2T_1 + 3T_2\right), \quad for\ i \neq j\ and\ i,j = 1,2,3 \tag{5}$$

These show that the lattice represents a cubic elasticity, which is not surprising as the complex is also a Voronoi diagram of body-centred cubic crystals. Notably the system is over-determined and allows for infinitely many choices for the inverse relations. One possibility, used in our applications, is to select $T_2 = 0$. With Voigt notations C_{11}, C_{12} and C_{44} for Eqns. (3), (4) and (5) respectively, this leads to Eq. (6) for springs in cubically elastic material. For isotropic material with Young's modulus E and Poisson's ratio ν, spring constants are given by Eq. (7).

$$K_1 = \frac{S}{2}\left(C_{44} + 2C_{12}\right); \quad T_1 = \frac{S}{2}\left(C_{44} - C_{12}\right); \quad K_2 = \frac{S}{2}\left(C_{11} - C_{44}\right) \tag{6}$$

$$K_1 = \frac{ES\left(1+2\nu\right)}{4\left(1+\nu\right)\left(1-2\nu\right)}; \quad T_1 = \frac{ES\left(1-4\nu\right)}{4\left(1+\nu\right)\left(1-2\nu\right)}; \quad K_2 = \frac{ES}{4\left(1+\nu\right)\left(1-2\nu\right)} \tag{7}$$

It can be seen that if spring stiffness coefficients were required to be positive, the lattice could represent all isotropic elastic materials with Poisson's ratio in the range $-0.5 \leq \nu \leq 0.25$, which is a substantial improvement from previous 3D lattices which allowed for isotropic elasticity with $\nu = 0$ only. It should be noted, however, that there is no conceptual problem with the extension for materials outside this interval. For $-1 < \nu < -0.5$ K_1 would become negative, and for $0.25 < \nu < 0.5$ T_1 would become negative. The use of negative stiffness may seem a violation of basic mechanics principles. However, it should be realized that the bond energy represents area energy on corresponding faces and the energy equivalence approach practically distributes the cell energy to 14 face energies in accordance with given kinematics. The area energies are not necessarily positive definite quadratic forms of strains as shown e.g. by Shenoy (2005) and Javili and Steinmann (2010). The spring constants correspond to coefficients of the surface stiffness tensor and hence need not be positive, as long as the total energy in the 14 bonds is positive. This proposition is a subject of ongoing work and will be reported in the future. Our current applications, Morrison et al. (2014b) and Zhang et al. (2014b), are to materials within the range $-0.5 \leq \nu \leq 0.25$.

3. Microstructure mapping

The correspondence between observable microstructure features and lattice properties is performed in statistical sense, since the cell complex represents topologically homogenised microstructure. We consider the solid as a continuum with internal free surfaces, e.g. voids or crack-like defects. The continuum is mapped to the interiors of the cell complex and may contain different solid phases. The internal free surfaces are mapped notionally to cell faces. In our current applications we consider two solid phases – a matrix of uniformly distributed matter and particles with different properties, e.g. density or structure, from the matrix. In such a case, the particles are placed at cell centres of the complex and the cell elasticity represents the averaged matrix-particle response. The construction of the corresponding site-bond model requires experimental data for the size distribution, $F(c)$, and volume density, θ_c, of particles. By distributing particles with sizes from the experimental distribution to a given

number of cells, N_c, and assuming spherical shapes, one can calculate the lattice length scale S for the prescribed particle volume fraction using Eq. (8). It should be noted that this process can be used to determine a representative volume element (RVE) for given $F(c)$ with respect to the lattice elastic response. By increasing N_c, the scatter in S for different random assignments of particles to cells for given θ_c is decreasing and the RVE can be assumed when the scatter is within prescribed limits, see Morrison et al. 2014a.

$$S = \sqrt[3]{\frac{8\pi}{4}\sum_{N_c} c_i^3 \Big/ N_c \theta_c} \tag{8}$$

Further, the model requires experimental data for the size distribution, $F(d)$, and volume density, θ_d, of defects. Presently, defects are assumed to be spherical pores, which are allocated with their great circle at faces of the complex to create the worst case scenario for initial face area reduction. The allocation is random spatially with sizes from $F(d)$ and terminates when the cumulative volume of the allocated pores reaches $V\theta_d$, where the total volume of the complex is $V = N_c\, S^3/2$ for selected N_c and calculated S. This is illustrated in Fig. 3. It should be noted that the mapping of crack-like defects could proceed in a similar way, but the required experimental data would be their number density in addition to size distribution. It is also worth mentioning that a model for a single solid phase can be constructed if volume and number density of pores were available, as these in combination could be used to calculate the length scale. In any case the defect mapping affects a set of faces, so that their initial areas, A_i, are reduced to effective areas $a_i = A_i - \pi d_i^2$. In the current applications, the effective areas dictate only bond failure properties as shown below, while the spring constants are calculated by Eq. (7) using macroscopic elastic properties measured on real material including porosity. Work is ongoing to include pore effects on spring constants, e.g. by a stiffness-effective area relation, and thus predict porosity effects on emergent elastic behaviour.

The bond failure mechanism is related to the matrix energy of separation, γ, a material parameter which can be determined either from lower (atomic) scale simulations, nano-indentation experiments or left for calibration against measured longer scale (continuum) response. Specific examples can be found in Morrison et al. (2014b) and Zhang et al. (2014b). The energy of separation defines bond failure energy as $G_i = \gamma a_i$, with $0 \le G_i \le \gamma A_i$ depending on the allocated pore area. Bond mechanical behaviour is shown schematically on Fig. 4, where F and u can be positive or negative, but specific to axial springs is that failure under compressive force is prohibited. The response to damage initiation point (F_c, u_c) is dictated by the initial spring constant K_i, followed by linear damage evolution to full separation at (0, αu_c). From the failure energy of a bond, G_i, the point (F_c, u_c) can be calculated for selected α, or α calculated for selected u_c (or F_c). Presently, $\alpha = 2$ is assumed to define full separation, until the softening behaviour is established more rigorously with lower scale simulations. It should be noted, however, that the described bond mechanical response will change once pore effects on spring constants are introduced.

The statistics of the microstructure features, required for the proposed modeling approach, is increasingly affordable with the wider availability of computed X-ray tomography; see Zhang et al. (2014b) for example.

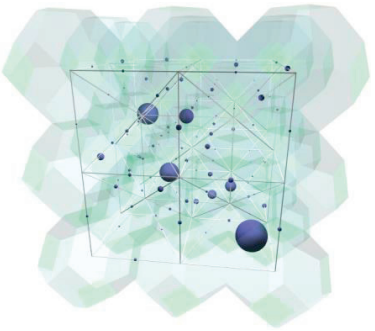

Fig. 3. Illustration of distributed pores on faces.

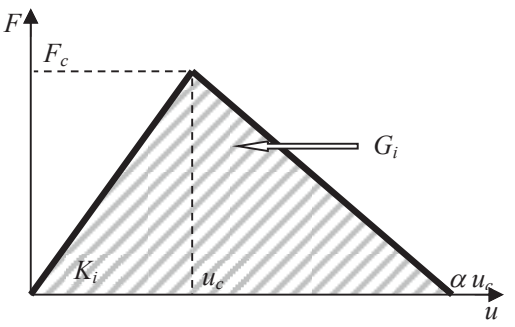

Fig. 4. Schematic spring mechanical behavior.

4. Discussion and conclusions

In this work we have introduced the basis for reduction of 3D continuum cell representation of materials to a 3D discrete lattice using a particular cell complex and applied this to justify mapping of material features to the discrete model. We have demonstrated that the proposed lattice can represent a large class of isotropic materials when springs with positive stiffness coefficients are used. In addition to this useful property, the cell complex allows for development of more realistic crack morphologies compared to previous lattices. This is very important since the main advantage of lattice models to continuum FEM formulations is the ability to generate and develop micro-cracks in a natural manner. We have further described how data from experimental characterisation can be used to obtain model parameters and discussed the need for further development. The model capabilities are demonstrated with specific examples in two contributions to this volume.

Acknowledgements

Jivkov and Zhang acknowledge gratefully the support from EPSRC via grant EP/J019763/1, "QUBE: Quasi-Brittle fracture: a 3D experimentally-validated approach", and from BNFL for the Research Centre for Radwaste & Decommissioning. Morrison acknowledges the support from EPSRC via Nuclear FiRST Doctoral Training Centre.

References

Aliha, M.R.M., Ayatollahi, M.R., 2012. Analysis of fracture initiation angle in some cracked ceramics using the generalized maximum tangential stress criterion. International Journal of Solids and Structures 49, 1877–1883.

Awaji, H., Matsunaga, T., Choi S.-M., 2006. Relation between Strength, Fracture Toughness, and Critical Frontal Process Zone Size in Ceramics. Materials Transactions 47, 1532–1539.

Ayatollahi, M.R., Aliha, M.R.M., 2011. Fracture Analysis of Some Ceramics Under Mixed Mode Loading. Journal of the American Ceramic Society 94, 561–569.

Carol, I., Jirasek, M., Bazant, Z., 2001. A thermodynamically consistent approach to microplane theory. Part I. Free energy and consistent microplane stress. International Journal of Solids and Structures 38, 2921-2931.

Cusatis, G., Pelessone, D., Mencarelli, A., 2011. Lattice discrete particle model (LDPM) for failure behaviour of concrete. I: Theory. Cement and Concrete Composites 33, 881-890.

Griffiths, D.V., Mustoe, G.G.W., 2001. Modelling of elastic continua using a grillage of structural elements based on discrete element concepts. International Journal for Numerical Methods in Engineering 50, 1759-1775.

Hadjesfandiari, A.R., Dargush, G.F., 2011. Couple stress theory for solids. International Journal of Solids and Structures 48, 2496-2510.

Javili, A., Steinmann, P., 2010. On thermomechanical solids with boundary structures. International Journal of Solids and Structures 47, 3245-3253.

Jivkov, A.P., Yates, J.R., 2012. Elastic behaviour of a regular lattice for meso-scale modelling of solids. International Journal of Solids and Structures 49, 3089-3099.

Jivkov, A.P., Hollis, C., Etiese, F., Withers, P.J., 2013a. A novel architecture for pore network modelling with applications to permeability of porous media. Journal of Hydrology 486, 246–258.

Jivkov, A.P., Engelberg, D.L., Stein, R., Petkovski, M., 2013b. Pore space and brittle damage evolution in concrete. Engineering Fracture Mechanics 110, 378-395.

Karihaloo, B.L., Shao, P.F., Xiao, Q.Z., 2003. Lattice modelling of the failure of particle composites. Engineering Fracture Mechanics 70, 2385-2406.

Liu, J.X., Zhao, Z.Y., Deng, S.C., Liang, N.G., 2009. Numerical investigation of crack growth in concrete subjected to compression by the generalised beam lattice model. Computational Mechanics 43, 277-295.

Morrison, C.N., Zhang, M., Jivkov, A.P., Yates, J.R., 2014a. A discrete lattice model of quasi-brittle fracture in porous graphite. Materials Performance and Characterization, in press, DOI: 10.1520/MPC20130077.

Morrison, C.N., Zhang, M., Jivkov, A.P., 2014b. Fracture energy of graphite from microstructure-informed lattice model.. 20th European Conference on Fracture, Trondheim, Norway, Paper #671.

Schlangen, E., van Mier, J.G.M., 1992. Experimental and numerical analysis of micromechanisms of fracture of cement-based composites. Cement and Concrete Composites 14, 105-118.

Shenoy, V.B., 2005. Atomistic calculations of elastic properties of metallic fcc crystal surfaces. Physical Review B 71, 094104.

Wang, Y., Mora, P., 2008. Macroscopic elastic properties of regular lattices. Journal of the Mechanics and Physics of Solids 56, 3459-3474.

Zhang, M., Morrison, C.N., Jivkov, A.P., 2014a. A meso-scale site-bond model for elasticity: Theory and calibration. Materials Research Innovations, in press.

Zhang, M., Morrison, C.N., Jivkov, A.P., 2014b. A lattice-spring model for damage evolution in cement paste. 20th European Conference on Fracture, Trondheim, Norway, Paper #675.